Monthly Notices
of the
ROYAL ASTRONOMICAL SOCIETY

MNRAS **462,** 1775–1785 (2016)
Advance Access publication 2016 July 30

doi:10.1093/mnras/stw1732

RoboPol: do optical polarization rotations occur in all blazars?

D. Blinov,[1,2,3★] V. Pavlidou,[1,2] I. Papadakis,[1,2] S. Kiehlmann,[4,5] I. Liodakis,[1,2] G. V. Panopoulou,[1,2] T. J. Pearson,[6] E. Angelakis,[7] M. Baloković,[6] T. Hovatta,[4,5] V. Joshi,[8] O. G. King,[6] A. Kus,[9] N. Kylafis,[1,2] A. Mahabal,[6] A. Marecki,[9] I. Myserlis,[7] E. Paleologou,[1,2] I. Papamastorakis,[1,2] E. Pazderski,[9] S. Prabhudesai,[8] A. Ramaprakash,[8] A. C. S. Readhead,[6] P. Reig,[1,2] K. Tassis[1,2] and J. A. Zensus[7]

[1]*Department of Physics and Institute for Plasma Physics, University of Crete, 71003 Heraklion, Greece*
[2]*Foundation for Research and Technology – Hellas, IESL, Voutes, 7110 Heraklion, Greece*
[3]*Astronomical Institute, St. Petersburg State University, Universitetsky pr. 28, Petrodvoretz, 198504 St. Petersburg, Russia*
[4]*Metsähovi Radio Observatory, Aalto University, Metsähovintie 114, FI-02540 Kylmälä, Finland*
[5]*Department of Radio Science and Engineering, Aalto University, PO Box 13000, FI-00076 Aalto, Finland*
[6]*Cahill Center for Astronomy and Astrophysics, California Institute of Technology, 1200 E California Blvd, MC 249-17, Pasadena, CA 91125, USA*
[7]*Max-Planck-Institut für Radioastronomie, Auf dem Hügel 69, D-53121 Bonn, Germany*
[8]*Inter-University Centre for Astronomy and Astrophysics, Post Bag 4, Ganeshkhind, Pune 411 007, India*
[9]*Toruń Centre for Astronomy, Nicolaus Copernicus University, Faculty of Physics, Astronomy and Informatics, Grudziadzka 5, PL-87-100 Toruń, Poland*

Accepted 2016 July 14. Received 2016 July 4; in original form 2016 April 19

ABSTRACT

We present a new set of optical polarization plane rotations in blazars, observed during the third year of operation of *RoboPol*. The entire set of rotation events discovered during three years of observations is analysed with the aim of determining whether these events are inherent in all blazars. It is found that the frequency of the polarization plane rotations varies widely among blazars. This variation cannot be explained either by a difference in the relativistic boosting or by selection effects caused by a difference in the average fractional polarization. We conclude that the rotations are characteristic of a subset of blazars and that they occur as a consequence of their intrinsic properties.

Key words: polarization – galaxies: active – galaxies: jets – galaxies: nuclei.

1 INTRODUCTION

Blazars are active galactic nuclei with relativistic jets oriented towards the observer. Relativistic boosting causes synchrotron radiation from the jet to dominate the blazar spectra at low frequencies (Blandford & Königl 1979). Consequently, the optical emission of blazars often has high and variable polarization. Commonly, the polarization fraction and the electric vector position angle (EVPA) in the optical band show irregular variations (e.g. Brindle et al. 1985). However, a number of events have been detected in which the EVPA traces continuous, smooth rotations that in some cases occur contemporaneously with flares in the total broad-band emission (Marscher et al. 2008).

It has been suggested that at least some large amplitude EVPA swings can be physically associated with gamma-ray flares (e.g. Larionov et al. 2013; Blinov et al. 2015; Zhang et al. 2016). The *RoboPol* programme[1] has been designed for efficient detection of EVPA rotations in statistically rigorously defined samples of gamma-ray-loud and gamma-ray-quiet blazars and to investigate possible correlations between their gamma-ray activity and optical EVPA variability (Pavlidou et al. 2014).

RoboPol started observations at Skinakas observatory, Greece, in 2013 May. The EVPA rotations detected during its first two years of operation were presented in Blinov et al. (2015, 2016, hereafter Papers I and II). In Paper I, we presented evidence that at least some EVPA rotations must be physically connected to the gamma-ray flaring activity. We also found that the most prominent gamma-ray flares occur simultaneously with EVPA rotations, while fainter flares may be non-contemporaneous with the rotations. This was taken as evidence for the co-existence of two separate mechanisms producing the EVPA rotations. In Paper II, we showed that the polarization degree decreases during the EVPA rotation events. The magnitude of this decrease is related to the rotation rate in the jet reference frame. Moreover we presented indications that the EVPA rotations cannot be of arbitrary duration and amplitude.

In this paper, we present a new set of EVPA rotations that were detected during the third *RoboPol* observing season in 2015. Then, using data from all three seasons we study the occurrence frequency

★ E-mail: blinov@physics.uoc.gr
[1] http://robopol.org

of the EVPA rotations in blazars. We aim to determine whether EVPA rotations occur in all blazars with the same frequency and to investigate whether the rotation events are related to the activity of the sources in the gamma-ray band.

2 OBSERVATIONS, DATA REDUCTION AND DETECTED EVPA ROTATIONS

The third *RoboPol* observing season started in 2015 May and lasted until the end of 2015 November. During this period we obtained more than 1200 measurements of objects from our monitoring sample. The sample is composed of three groups: the main ('gamma-ray-loud') group of 62 blazars detected by *Fermi*-Large Area Telescope (LAT) and listed in the 2FGL catalogue (Nolan et al. 2012); a control group of 17 'gamma-ray-quiet' blazars; and an additional group of 24 sources of high interest [see Pavlidou et al. (2014) for details of the sample selection]. The control sample originally included 15 sources, but two of them have been detected by *Fermi*-LAT since the start of our project and are listed in the 3FGL catalogue (Acero et al. 2015). We therefore included these two sources, which had not been detected previously by *Fermi*-LAT, in the main sample for the third observing season.

2.1 Observations and data reduction

All the polarimetric data analysed in this paper were obtained at the 1.3-m telescope of Skinakas observatory using the *RoboPol* polarimeter. The polarimeter was specifically designed for this monitoring programme. It has no moving parts besides the filter wheel and thus avoids unmeasurable errors caused by sky changes between measurements and the non-uniform transmission of a rotating optical element. The instrument and the specialized pipeline with which the data were processed are described in King et al. (2014).

The data were taken in the *R* band. Magnitudes were calculated using calibrated field stars either found in the literature[2] or presented in the Palomar Transient Factory catalogue (Ofek et al. 2012). Photometry of blazars with bright host galaxies was performed with a constant 4 arcsec aperture. All other sources were measured with an aperture defined as 2.5 × FWHM, where FWHM is the average full width at half-maximum of stellar images in the 13 × 13 arcmin field and has a median value of 2.1 arcsec.

The exposure time was adjusted according to the brightness of each target, which was estimated during a short pointing exposure. Typical exposures for targets in our sample were in the range 2–30 min. The average relative photometric error was ∼0.04 mag. Objects in our sample have Galactic latitude $|b| > 10^\circ$, so the average colour excess in the directions of our targets is relatively low, $\langle E(B-V)\rangle = 0.11$ mag (Schlafly & Finkbeiner 2011). Consequently, the interstellar polarization is expected to be less than 1.0 per cent on average (Serkowski, Mathewson & Ford 1975). The statistical uncertainty in the measured degree of polarization is less than 1 per cent in most cases, while the EVPA is typically determined with a precision of 1°–10° depending on the source brightness and fractional polarization.

We resolve the 180° EVPA ambiguity by assuming that the temporal variation is smooth and does not exceed 90° between two consecutive measurements θ_n and θ_{n+1}. The variation is defined as $\Delta\theta = |\theta_{n+1} - \theta_n|$ and considered to be significant if $\Delta\theta > \sqrt{\sigma(\theta_{n+1})^2 + \sigma(\theta_n)^2}$, where $\sigma(\theta_i)$ is the uncertainty of θ_i. If $\Delta\theta - \sqrt{\sigma(\theta_{n+1})^2 + \sigma(\theta_n)^2} > 90^\circ$, we shift the angle θ_{n+1} by $\pm k \times 180^\circ$, where the integer $\pm k$ is chosen in such a way that it minimizes $\Delta\theta$. Otherwise, we leave θ_{n+1} unchanged.

[2] https://www.lsw.uni-heidelberg.de/projects/extragalactic/charts/

2.2 Detected EVPA rotation events

Following Papers I and II, we define an EVPA rotation as any continuous change in the EVPA that is indicated by at least four consecutive measurements with at least three significant swings between them, and has a total amplitude of $\Delta\theta_{\rm max} \geq 90^\circ$. Moreover, the EVPA curve slope $\Delta\theta_i/\Delta t_i$ has to change by no more than a factor of 5 between consecutive pairs of measurements, and must preserve its sign.

In the data set obtained during the 2015 observing season we identified 13 events in 10 blazars of the main sample that satisfy our definition of an EVPA rotation. The full season EVPA curves along with the evolution of the polarization degree and the *R*-band flux density, for the 10 blazars with detected rotations, are shown in Fig. 1. The EVPA rotation intervals are marked by the filled circles. The observational parameters of the rotations: the amplitude, $\Delta\theta_{\rm max}$, and the average rate, $\langle\Delta\theta/\Delta T\rangle$, are listed in Table 1, along with the observing season length, $T_{\rm obs}$, and the median cadence of observations, $\langle\Delta t\rangle$, for the corresponding blazar. The EVPA swing event in RBPL J0136+4751 might be considered to be a single rotation, but according to our definition it is composed of two successive rotations separated by a significant swing in the opposite direction to the global trend.

3 FREQUENCY OF EVPA ROTATIONS IN BLAZARS

During the 2013–2015 observing seasons we detected 40 EVPA rotation events in 24 blazars (see Papers I and II for details of the first two seasons). Two events reported in Paper I belong to neither the main nor the control sample. Two more events from Paper I do not follow our definition of an EVPA rotation strictly. These four events will not be taken into account in the analysis below. Using the remaining 36 rotations, in the following sections we address the question: do *all* blazars show EVPA rotations in the optical band?

3.1 Main and control sample blazars as a single population

A major advantage of the *RoboPol* project is that it was operated in such a way that the objects in the two samples would be observed in a 'similar' way. Nevertheless, the median observing cadence, $\langle\Delta t\rangle$, and the season length, $T_{\rm obs}$, are not identical for all the blazars that we monitored. In Fig. 2 we show $\langle\Delta t\rangle$ versus $T_{\rm obs}$ for each object we observed during each of the observing seasons. The lines in Fig. 2 bound regions ('detection boxes') in the $\langle\Delta t\rangle - T_{\rm obs}$ plane where a rotation slower than a given rate could have been detected for each object within the area (see section 3.3 of Paper I for details). For example, the dashed line in Fig. 2 indicates the maximum $\langle\Delta t\rangle$ value for a given duration of observations, $T_{\rm obs}$, that is needed to detect rotations with a rate of $\langle\Delta\theta/\Delta T\rangle \leq 7$ deg d^{-1}. We are confident that we can detect rotations with $\langle\Delta\theta/\Delta T\rangle < 7$ deg d^{-1} for all the blazars within the 7 deg d^{-1} detection box. The solid and the dash–dotted lines in Fig. 2 show the 10 and 20 deg d^{-1} detection boxes, respectively.

In order to compare the EVPA rotation frequencies in blazars that belong to different sub-samples, we need to consider data from sources in the same detection boxes. The choice of the rotation rate

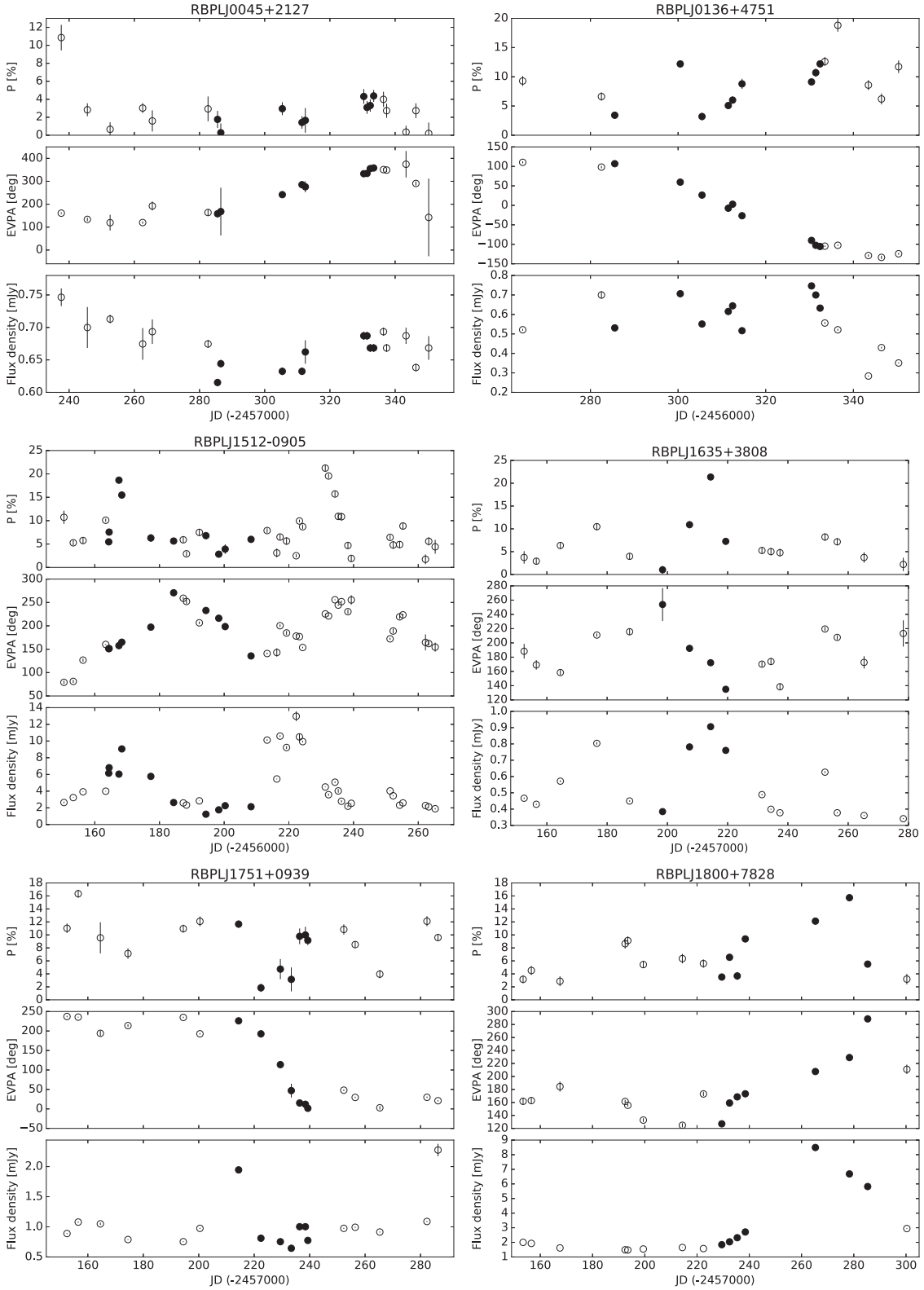

Figure 1. Evolution of fractional polarization, EVPA and *R*-band flux density for blazars with rotations detected during the third *RoboPol* season. Periods of rotations are marked by filled circles.

limit is a trade-off between the number of sources within the detection box and the investigation of a wider range of EVPA rotation rates. For example, the choice of 7 deg d^{-1} allows us to use data from a number of sources that is substantially larger than the number of sources that are 'complete' in the detection of rotations with a rate of $\leq$20 deg d^{-1}, although the latter encompasses a larger portion of all possible EVPA rotation events. In the analysis below, we consider the objects in all three detection boxes as much as possible.

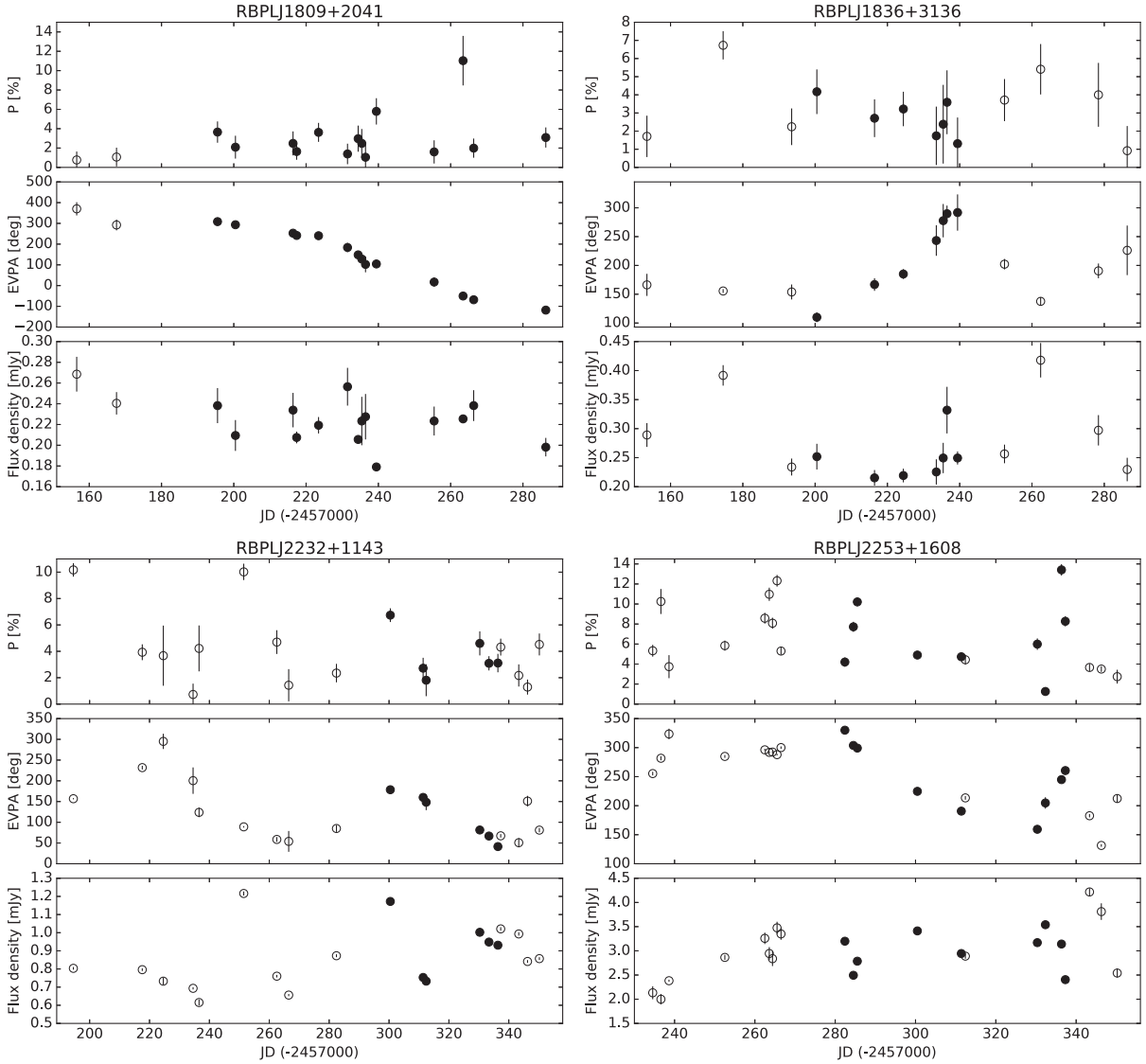

Figure 1 – *continued*

Table 1. Observational data for the EVPA rotations detected by *RoboPol* in 2015. Columns (1) and (2): blazar identifiers; (3): 2015 observing season length; (4): median time difference between consecutive observations; (5): total amplitude of EVPA change; (6): duration of the rotation; (7): number of observations during rotation; (8): average rotation rate.

Blazar ID	Survey name	$T_{\rm obs}$ (d)	$\langle\Delta t\rangle$ (d)	$\Delta\theta_{\rm max}$ (deg)	$T_{\rm rot}$ (d)	$N_{\rm rot}$	$\langle\Delta\theta/\Delta T\rangle$ (deg d^{-1})
RBPL J0045+2127	GB6 J0045+2127	113	3.0	199.8	48	9	4.2
RBPL J0136+4751	OC 457	86	3.0	−114.2	26	4	−4.4
RBPL J0136+4751	−″−	−″−	−″−	−108.5	20	5	−5.4
RBPL J1512−0905	PKS 1510−089	115	2.0	119.6	20	6	6.0
RBPL J1512−0905	−″−	−″−	−″−	−97.2	14	4	−7.0
RBPL J1635+3808	4C 38.41	126	9.0	−118.9	21	4	−5.7
RBPL J1751+0939	OT 081	134	7.0	−224.5	25	7	−9.0
RBPL J1800+7828	S5 1803+784	147	7.5	161.6	56	7	2.9
RBPL J1809+2041	RX J1809.3+2041	130	6.0	−426.7	91	14	−4.7
RBPL J1836+3136	RX J1836.2+3136	133	9.0	181.8	39	7	4.7
RBPL J2232+1143	CTA 102	156	6.5	−137.1	36	6	−3.8
RBPL J2253+1608	3C 454.3	116	2.0	−139.4	29	5	−4.8
RBPL J2253+1608	−″−	−″−	−″−	101.2	7	4	14.5

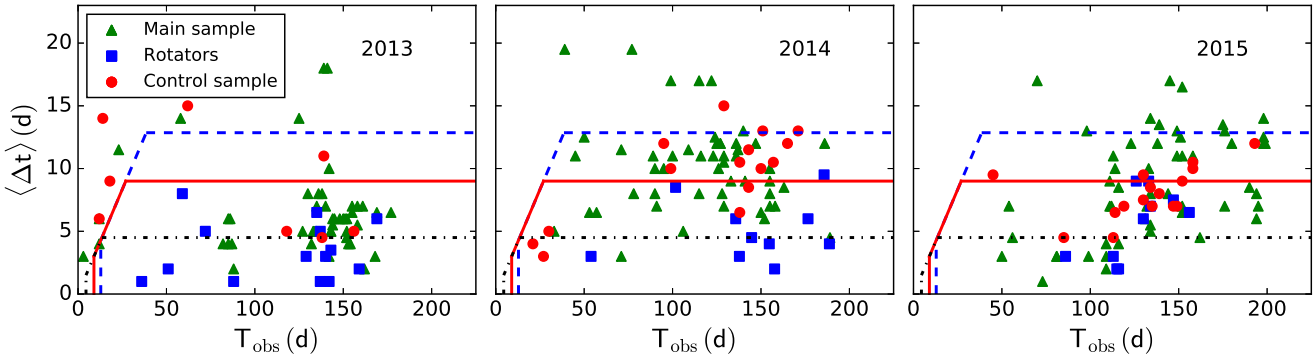

Figure 2. Season length, $T_{\rm obs}$, and median cadence, $\langle\Delta t\rangle$, for blazars with detected rotations for all observing seasons. The lines border areas inside which rotations slower than 7 (dashed blue), 10 (solid red) and 20 deg d^{-1} (dot–dashed black) can be detected (see the text for details).

Table 2. Estimates of rotations frequencies. Columns (1) – total number of rotations; (2) – summed observing length; (3) – average frequency of rotations; (4) – probability of observing $N_{\rm rot}$ during $T_{\rm obs}$ if all blazars have equal frequency of rotations $\lambda_{\rm all}$.

	$N_{\rm rot}$	$T_{\rm obs}$ (d)	λ (d^{-1})	$\mathcal{P}$
		≤ 7 deg d^{-1}		
All:	22	24 584	8.9×10^{-4}	–
Rotators:	22	6296	(3.5×10^{-3})	1×10^{-7}
Non-rotators:	0	18 288	$(<5.5 \times 10^{-5})$	9×10^{-8}
		≤ 10 deg d^{-1}		
All:	24	17 820	1.4×10^{-3}	–
Rotators:	24	5847	(4.1×10^{-3})	4×10^{-6}
Non-rotators:	0	11 973	$(<8.4 \times 10^{-5})$	5×10^{-8}
		≤ 20 deg d^{-1}		
All:	20	5412	3.7×10^{-3}	–
Rotators:	20	2224	(9.0×10^{-3})	2×10^{-4}
Non-rotators:	0	3188	$(<3.1 \times 10^{-4})$	8×10^{-6}

Columns 1 and 2 in Table 2 list the number of detected rotations, $N_{\rm rot}$, slower than the given rate and the total observing length, $T_{\rm obs}$, for all blazars within the 7, 10 and 20 deg d^{-1} detection boxes. For instance, the top panel in Table 2 takes into account only sources located within the 7 deg d^{-1} detection boxes for all three seasons, and rotations only with a rate of $\leq$7 deg d^{-1}. Column 3 gives the average frequency of rotations, λ, slower than the given rate. This frequency is defined as $\lambda = N_{\rm rot}/T_{\rm obs}$, for $N_{\rm rot} > 0$. In the case of $N_{\rm rot} = 0$, we list an upper limit on λ, which is defined as $1/T_{\rm obs}$. The corresponding numbers are listed separately for blazars with and without detected EVPA rotations (rotators and non-rotators hereafter). From the table we can see that λ differs by more than an order of magnitude between rotators and non-rotators.

The probability that n independent events occur in a period of time t can be estimated using the Poisson distribution,

$$\mathcal{P}(n, t, \lambda) = \frac{(\lambda t)^n}{n!} e^{-\lambda t}, \quad (1)$$

where λ is the average frequency of the events. Then, using data from Table 2, under the hypothesis that *all blazars exhibit rotations with equal frequency*, we can estimate the probability of having $N_{\rm rot}$ rotations in blazars that were observed over a period of time $T_{\rm obs}$. For instance, the probability of having 22 rotations slower than 7 deg d^{-1} in blazars that fall in the corresponding detection boxes in Fig. 2 and were observed for 6296 d is $\mathcal{P}(22, 6296, 8.9 \times 10^{-4}) = 1 \times 10^{-7}$. This result indicates that, under the hypothesis of the same frequency of rotations in blazars, it is highly unlikely to detect such a large number of rotations in a small number of objects observed in such a short $T_{\rm obs}$.

Following the same reasoning we found the corresponding probabilities, $\mathcal{P}$, for rotators and non-rotators within the three detection boxes. These probabilities, presented in Column 4 of Table 2, are less than 2×10^{-4} in all cases. Therefore, the null hypothesis is rejected at a high significance level for all detectable rotation rates: *it is highly unlikely that all blazars exhibit rotations of the polarization plane with rates* $\leq$20 deg d^{-1}*, with the same frequency*.

3.2 Absence of rotations in the control sample

If EVPA rotations are related to the gamma-ray activity of blazars, the low probabilities we found in the previous section may perhaps arise from the fact that we considered both gamma-ray-loud and gamma-ray-quiet sources as a single population in the analysis above. Here we test whether the two classes of blazars differ significantly in the frequency of EVPA rotation they exhibit.

As shown in the previous section, 22 rotations occurred in blazars that are located within the 7 deg d^{-1} detection boxes and have rates slower than 7 deg d^{-1}. The total observing length for the main sample blazars in the 7 deg d^{-1} detection boxes for all three seasons is 20 625 d. Thus we can estimate the frequency of rotations with $\langle\Delta\theta/\Delta T\rangle < 7$ deg d^{-1} in the main sample sources as one rotation in $\sim$940 d ($T_{\rm obs} = 20\,625$ d$/N_{\rm rot} = 22$ rotations). Following the same rationale we estimate average frequencies of rotations with rates $\leq$10 deg d^{-1} and $\leq$20 deg d^{-1} as one rotation in $\sim$650 d (15 632/24) and $\sim$250 d (5028/20).

The total $T_{\rm obs}$ for the control sample blazars lying within the 7 deg d^{-1} detection boxes in Fig. 2 is 3959 d. Under the hypothesis that *blazars of the control sample show EVPA rotations with the same frequency as the main sample sources*, we can estimate the probability of not detecting any rotation with $\langle\Delta\theta/\Delta T\rangle < 7$ deg d^{-1} in the control sample blazars, as $\mathcal{P}(0, 3959, 1/940) = 1.5$ per cent. Similarly, the probability of not detecting rotations slower than 10 and 20 deg d^{-1} in the control sample is 3.5 per cent and 22 per cent, respectively. These numbers imply that we cannot reject the null hypothesis at a sensibly significant level; it is possible that λ is the same for the blazars in the main and the control samples.

These results indicate that the highly significant difference in the frequency of the EVPA rotations in the rotators and non-rotators

Table 3. Frequencies of EVPA rotations in the main sample sources within the 7 deg d^{-1} detection box. Columns (1) – total number of rotations; (2) – summed observing period length; (3) – average frequency of rotations.

	$N_{\rm rot}$	$T_{\rm obs}$ (d)	λ (d^{-1})
0 rotations	0	129 78	$<7.7 \times 10^{-5}$
1 rotation	12	4462	2.7×10^{-3}
2 rotations	6	1246	4.8×10^{-3}
3 rotations	6	885	6.8×10^{-3}
4 rotations	12	1054	1.1×10^{-2}
All rotators:	36	7647	4.7×10^{-3}
Total:	36	20 625	1.8×10^{-3}

is not due to the fact that we did not observe any rotations in the control sample blazars. The majority of the main sample blazars did not show any rotations either. It is possible then that the rate of EVPA rotations is not constant even among the blazars of the main sample. We investigate this possibility in the following section.

3.3 Subclasses of blazars within the main sample

In this section, we ascertain whether the occurrence of EVPA rotations in the blazars of the main sample is consistent with a single population of sources that exhibit rotations with equal frequency. For this purpose we separate the main sample into five sub-samples: blazars that did not show any rotation, and blazars that had one to four rotations during the whole observing period. Then, for each group, we count the total number of rotations, $N_{\rm rot}$, the total observing period length, $T_{\rm obs}$, and the average frequency of rotations, λ, as defined earlier, using the sources within the 7 deg d^{-1} detection boxes in Fig. 2. These data are presented in Table 3. The average frequency of rotations is strongly non-uniform among the sub-samples. The frequency of rotations λ in non-rotators of the main sample is more than two orders of magnitude smaller than λ for the blazars that exhibited four events.

A number of hypotheses can be considered to verify whether the difference of λ for these sub-groups of blazars is accidental or not. Under the null hypothesis that *all blazars of the main sample represent a single class and exhibit EVPA rotations with the average frequency of* $\lambda = 1.8 \times 10^{-3}$ d^{-1}, using equation (1) we find the probability of detecting zero rotations in 41 sources observed for 12 978 d is $\mathcal{P}(0, 12978, 1.8 \times 10^{-3}) = 7.2 \times 10^{-11}$. On the other hand, if we assume that *all blazars have the same frequency of rotations equal to* $\lambda = 7.7 \times 10^{-5}$ d^{-1} (this is the upper limit of the frequency of rotations for the non-rotators of the main sample), then the probability of detecting 36 events in the whole sample during 20 625 d of observations is $\mathcal{P}(36, 20625, 7.7 \times 10^{-5}) = 9 \times 10^{-36}$. Moreover, assuming that the average frequency of rotations $\lambda = 4.7 \times 10^{-3}$ d^{-1} is characteristic of all rotators, we find the probability of detecting 12 rotations in the group of 3 blazars each of those exhibited 4 rotations as $\mathcal{P}(12, 1054, 4.7 \times 10^{-3}) = 3.2 \times 10^{-3}$. We therefore conclude that *the frequency of the EVPA rotations is significantly different among blazars of the main sample*.

The analysis above implies that there is a sub-class of objects that exhibit EVPA rotations much more frequently than others. This difference does not simply depend on whether or not a blazar is detected by *Fermi*-LAT. Even in objects that are in our gamma-ray-loud sample and did not show any rotation, the frequency of the EVPA rotations must be significantly smaller than the frequency exhibited by the rotators in our sample.

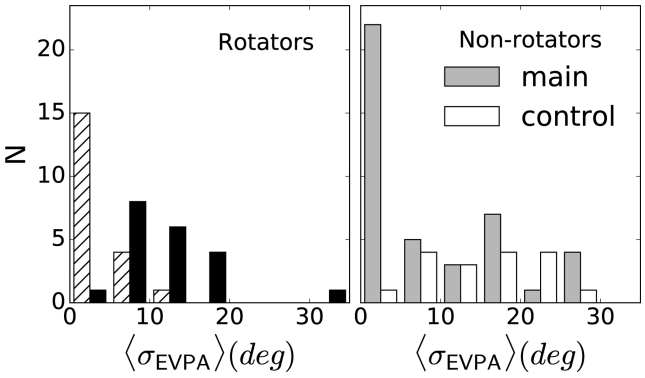

Figure 3. Distribution of the median measured uncertainty of the EVPA measurements. Left-hand panel: uncertainties in the rotator sub-sample, measured (hatched bars), and multiplied by a factor of 4 (black bars). Right-hand panel: uncertainties in the non-rotators of the main sample and the control sample.

4 POSSIBLE REASONS OF DIFFERENT OBSERVED ROTATION FREQUENCIES

The analysis presented above uses data from objects with the same sampling properties in their light curves. However, there are two more observational factors which may bias our results and conclusions. The first one depends on possible differences in the accuracy with which we can measure EVPA in rotators and non-rotators. The second is related to possible intrinsic differences in the rest-frame properties, namely redshift, z, and Doppler factor, δ, of rotators and non-rotators. We address both issues below.

4.1 Differences in accuracy of EVPA measurements

It has been shown by Pavlidou et al. (2014) and Angelakis et al. (in preparation) that the control sample blazars are on average significantly less polarized than the main sample blazars. This could potentially be the reason for the absence of EVPA rotation detections in the control sample. Our definition of an EVPA rotation requires three or more significant swings between four or more consecutive EVPA measurements. Lower fractional polarization leads to higher uncertainties in the EVPA, so larger errors may hide significant swings. If non-rotators are significantly less polarized than rotators we might have missed rotations in their EVPA curves because of this observational bias.

One way to address this issue is to compare the mean polarization fraction of rotators and non-rotators. Here we choose to investigate this issue directly, i.e. we compare the amplitude of the EVPA error in rotators and non-rotators. The distribution of the median uncertainty, $\langle\sigma_{\rm EVPA}\rangle$, of the EVPA measurements for the rotators and not-rotators is shown in the left- and the right-hand panels of Fig. 3. The hatched, grey and white bars correspond to rotators, non-rotators of the main sample, and non-rotators of the control sample. On average, $\langle\sigma_{\rm EVPA}\rangle$ of non-rotators is larger than $\langle\sigma_{\rm EVPA}\rangle$ of rotators. A number of non-rotators in the main sample show small uncertainties, but all the control sample sources and quite a few of the main sample non-rotators show large uncertainties. The two-sample Kolmogorov–Smirnov (K–S) test rejects the hypothesis that the $\langle\sigma_{\rm EVPA}\rangle$ distribution of rotators and non-rotators (all together) is sampled from the same parent population (p-value $= 3 \times 10^{-4}$).

However, we do not believe that this difference is the main reason why we do not detect rotations in the non-rotators. To demonstrate this, we multiplied $\sigma_{\rm EVPA}$ of each measurement in the EVPA curves

of rotators by a factor f. The distribution of $\langle\sigma_{\rm EVPA}\rangle$ for the rotators when $f = 3$ is shown by the black bars in the left-hand panel of Fig. 3. The null hypothesis that this distribution and the distribution of $\langle\sigma_{\rm EVPA}\rangle$ for the control sample are drawn from the same parent population cannot be rejected according to the K–S test (p-value = 0.03). More than half of the rotations (22 out of 36) still follow our definition of an EVPA rotation for $f = 3$.

In order to investigate the significance of the measurement accuracy, we repeated the analysis performed in Section 3.1 for rotators and non-rotators within the 7 deg d^{-1} detection box, ignoring the 14 events that do not follow our definition of an EVPA rotation when $f = 3$. Among the remaining rotations that follow the definition, 13 events have rates slower than 7 deg d^{-1}. Therefore, the frequency of rotations decreases in this case, from $\lambda = 22/24\,584 = 8.9 \times 10^{-4}$ d^{-1}, to $\lambda = 13/24\,584 = 5.3 \times 10^{-4}$ d^{-1}. However, even in this case, according to equation (1), the probability of detecting 13 rotations in blazars observed for 3589 d is $\mathcal{P}(13, 3589, 5.3 \times 10^{-4}) = 10^{-7}$. Similarly, the probability of not detecting any rotations in the remaining blazars observed for 20 995 d is $\mathcal{P}(0, 20995, 5.3 \times 10^{-4}) = 2 \times 10^{-5}$. Thus even when we artificially increase the uncertainty of EVPA measurements in rotators in such a way that $\langle\sigma_{\rm EVPA}\rangle$ distributions for rotators and non-rotators become comparable, the frequency of rotations cannot be the same for the two groups.

Therefore the difference in the amplitudes of the EVPA uncertainties could partially explain the absence of detected rotations in non-rotators. However, it is not large enough to be entirely responsible for the difference in the frequencies of EVPA rotations between rotators and non-rotators found in Section 3.

4.2 Rest frame time-scale differences

Another possible explanation for the variation in rotation frequency is that we miss rotations in some blazars because the duration of observations in the jet rest frame, $T^{\rm jet}_{\rm obs}$, may be significantly different for the rotators and the non-rotators. The analysis in Section 3 is based on the total number of observing days in the observer frame, $T_{\rm obs}$, for the rotators and non-rotators. The jet frame and the observer frame time-scales are related as $\Delta T^{\rm jet} = \Delta T^{\rm obs}\delta/(1+z)$. Therefore, $T^{\rm jet}_{\rm obs}$ depends on the Doppler factor, δ, and the redshift, z, of the sources as well. If the δ and/or z distributions are significantly different for rotators and non-rotators then the difference in λ found above could be artificial.

Table A1 lists estimates of δ and z for the blazars in our sample taken from the literature. We use δ values estimated from the variability of the total flux density in the radio band, which are believed to be the most reliable and self-consistent Doppler factor estimates available[3] (Liodakis & Pavlidou 2015). Such estimates are available for 21 sources in both samples. Fig. 4 shows the distribution of these δ values for rotators and non-rotators. The null hypothesis that the two distributions are drawn from the same population is strongly supported by the data according to the K–S test (p-value = 0.62).

Redshift estimates are available for 71 sources in the two samples; 52 are based on optical spectroscopic data, while the other 19 are obtained using indirect methods (broad-band photometry of the host galaxies, attenuation of the hard gamma-ray emission, etc.). According to the K–S test the null hypothesis that the distributions

[3] The actual Doppler factors for the optical emission region may be significantly different, but estimates are not available at the moment.

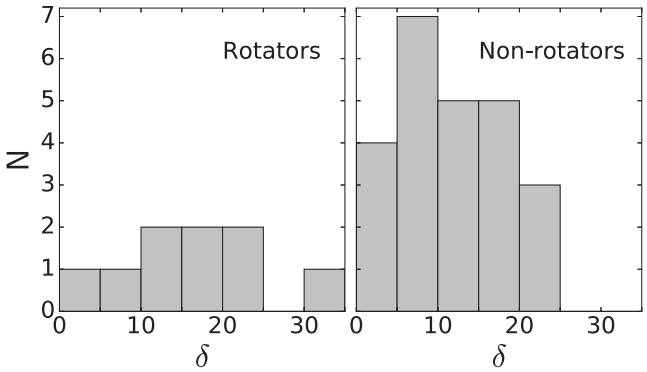

Figure 4. Distribution of δ for rotators and non-rotators.

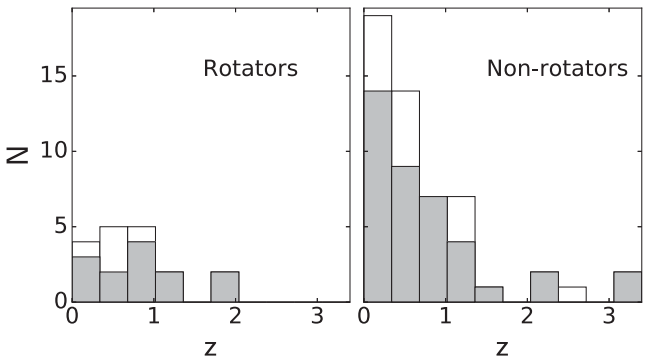

Figure 5. Distribution of z for rotators and non-rotators. Grey bars include only spectroscopic z estimates, white bars include indirect z estimates.

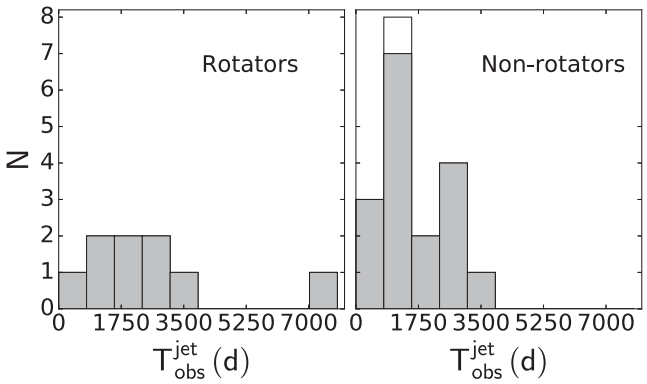

Figure 6. Distribution of $T^{\rm jet}_{\rm obs}$ for rotators and non-rotators. Grey bars include only spectroscopic z estimates, white bars include indirect z estimates.

of z for rotators and non-rotators (Fig. 5) are drawn from the same population cannot be rejected (p-value = 0.48 for the spectroscopic, and 0.54 for all available redshifts).

For the blazars with known δ and z that are located in the 7 deg d^{-1} detection boxes in Fig. 2, we computed the total $T_{\rm obs}$ and transformed it to the jet frame $T^{\rm jet}_{\rm obs}$. The $T^{\rm jet}_{\rm obs}$ distributions for rotators and non-rotators are shown in Fig. 6. According to the K–S test, the hypothesis that $T^{\rm jet}_{\rm obs}$ for rotators and non-rotators are drawn from the same population is again supported by the data (p-value = 0.27 for spectroscopic, and 0.25 for all available redshifts).

Using the reasoning of Section 3 we can estimate how large the difference between the average Doppler factors of the rotators and the non-rotators must be to explain the absence of rotations in the EVPA curves of non-rotators. According to equation (1) and

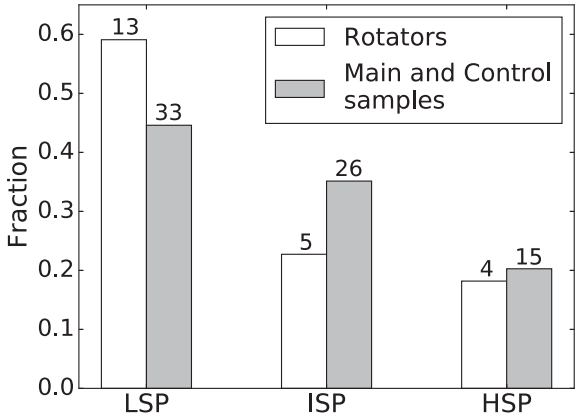

Figure 7. Distribution of blazars in the main and control samples together and rotators among the synchrotron peak position types. Fraction is calculated as the number of sources of a given synchrotron peak class divided by the total number of sources in the corresponding sample.

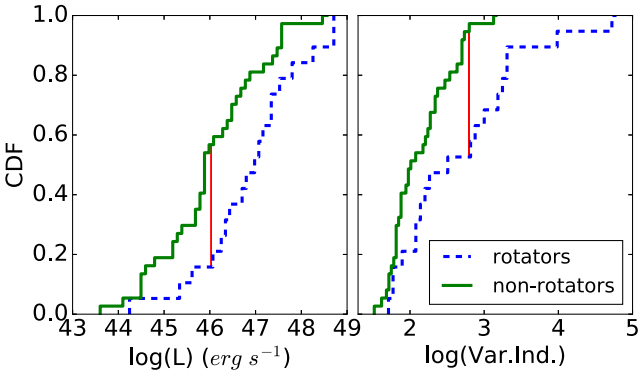

Figure 8. CDF of luminosity (left) and variability index (right) for rotators and non-rotators. The red vertical line indicates the maximum difference between the CDFs.

the frequency estimate for rotations slower than 7 deg d^{-1} from Section 3.1, if we reduce the total $T_{\rm obs}$ for non-rotators by a factor of 4, then the probability of having zero rotations in this sub-sample of blazars can reach $\sim$1 per cent. This means that if the average Doppler factor for the non-rotators was four times smaller than that of the rotators, then the absence of rotations could be an accidental outcome of the Poisson distribution of the rotations. Such a large difference is inconsistent with the aforementioned K–S test that finds no difference in the distributions of $\delta/(1+z)$ for rotators and non-rotators.

In summary, our analysis strongly suggests that there exists a sub-class of blazars that exhibit EVPA rotations in the optical band significantly more frequently than the others. The difference in the frequency of the rotations cannot be explained by the non-uniformity of observations or by observational biases due to differences in the average fractional polarization. Moreover, based on the available data, it cannot be explained by differences in the relativistic beaming or in the redshifts between the rotators and non-rotators. In the next two sections we investigate possible physical reasons that might be responsible for the prevalence of the optical EVPA rotations in this sub-class of blazars.

5 ROTATIONS IN BLAZARS OF DIFFERENT CLASSES

In this section, we examine whether the ability of a blazar to exhibit EVPA rotations depends on its synchrotron peak location. The classification as either a low-, intermediate- or high-synchrotron-peaked (LSP, ISP or HSP) blazar for the main sample sources was taken from the third catalogue of active galactic nuclei detected by the *Fermi*-LAT (3LAC, Ackermann et al. 2015). For the control sample sources, which are not in 3LAC, the synchrotron peak positions were taken from Angelakis et al. (in preparation) and Mao et al. (2016), where a procedure similar to the one used by Ackermann et al. (2015) was applied. The classification of blazars in our sample according to the synchrotron peak position is listed in Table A1. We find that the main and the control samples together are composed of 33 LSP, 26 ISP and 15 HSP sources. The sample of rotators is composed of 13 LSP, 5 ISP and 4 HSP sources. The distribution of the sources among the classes is shown in Fig. 7. We estimate the probability that rotators comprise sources randomly drawn from the main and the control samples together as:

$$\mathcal{P} = \frac{C_{33}^{13} C_{26}^{5} C_{15}^{4}}{C_{74}^{22}} = 0.014, \quad (2)$$

where C_n^k is the binomial coefficient. The numerator in this equation is the number of ways to obtain a sample composed of 13 LSP, 5 ISP and 4 HSP blazars from the parent sample of 33 LSP, 26 ISP and 15 HSP sources. The denominator is the total number of combinations how 22 objects can be selected out of 74. Similarly, the probability that rotators are randomly drawn from the main sample only is 0.5 per cent. Therefore it is unlikely that LSP accidentally dominate over ISP and HSP among the blazars that exhibit rotations.

6 GAMMA-RAY PROPERTIES OF ROTATORS AND NON-ROTATORS

As demonstrated in Section 3.3, the rotators form a particular sub-sample of objects even among the sources in our main sample. In this section, we investigate whether there are any differences in the gamma-ray properties between these two sub-classes. To this end, we extract the variability indices and we calculate luminosities in the gamma-ray band (100 MeV $\leq E \leq$ 100 GeV) for blazars of our main sample using the data from the 3FGL catalogue (Acero et al. 2015). The cumulative distribution functions (CDFs) of these quantities for rotators and non-rotators are shown in Fig. 8. According to the two-sample K–S test there is a strong indication that both luminosity (p-value = 0.02) and variability (p-value = 0.01) are higher for the blazars that exhibited rotations.

This is presumably caused by the dominance of LSP sources among rotators found in the previous section, since LSP blazars tend to have higher gamma-ray luminosities than HSP sources (Ackermann et al. 2015). High variability indices in the gamma-ray band are characteristic of sources that are both luminous and variable (Ackermann et al. 2015). Therefore the difference in the variability indices is also explained by the dominance of LSP blazars among the rotators.

7 DISCUSSION AND CONCLUSIONS

We have presented a set of EVPA rotations detected by *RoboPol* during the 2015 observing season. After three years of operation we have detected 40 EVPA rotations, and thereby more than tripled the list of known events of this type.

Our monitoring sample was constructed on the basis of statistically robust and bias-free criteria. It included both gamma-ray-loud and gamma-ray-quiet blazars that were monitored with equal cadence. This allowed us to perform statistical studies of the frequency of EVPA rotations in blazars for the first time.

We have shown that the frequency of rotations varies significantly among blazars. None of the control sample blazars displayed a rotation during the monitoring period. Moreover, the EVPA rotations occur with significantly different frequency in different blazars in the main sample. There is a subset of blazars that show the events much more frequently than others. This result is consistent with our analysis in Paper I, where we showed that rotators have higher EVPA variability than non-rotators even outside the rotating periods.

This is a major result of the *RoboPol* project: only a fraction of blazars (∼28 per cent of sources in both samples) exhibit EVPA rotations with rates $\leq$20 deg d^{-1} in the optical band, with an average frequency of 1/232 d^{-1} (in the observer frame). The remaining ∼72 per cent of sources did not show any rotations. If they do exhibit rotations, this should happen with a frequency less than ∼1/3230 d^{-1}.

The analysis of Section 4 shows that the difference in the frequencies of EVPA rotations cannot be explained either by the difference in the EVPA measurement uncertainties or by differences in redshifts and/or Doppler factors among the blazars. This result should be confirmed using a larger number of objects with known δ. Only a small fraction of blazars in our monitoring sample have Doppler factor estimates available. The ongoing analysis of variability in the radio band will allow us to increase the sample of blazars with known Doppler factors and allow us to verify our results with better statistics.

The tendency for EVPA rotations to occur in LSP blazars found in Section 5 can be explained in the same way as higher variability of LSP sources in the total optical flux. It has been shown by Hovatta et al. (2014) that LSP blazars are more variable than HSP in the optical band. This was attributed to the fact that, in the optical band, LSP sources are observed near their electron energy peak, which causes stronger variations of the emission compared to HSP sources, where the lower energy electrons cool down slowly and produce mild variability. For the same reason, the polarized flux density as well as the EVPA must be more variable in LSP sources compared to HSP when observed in the optical band. If this interpretation is correct, then HSP blazars must exhibit EVPA rotations more frequently at higher frequencies (UV and X-ray bands). The dependence of the optical EVPA behaviour on the synchrotron peak position is also reported in two other papers based on RoboPol data. Angelakis et al. (2016) have shown that the EVPA in HSP sources centres around a preferred direction, while in LSP blazars it follows a more uniform distributions. Hovatta et al. (2016) have shown that the scatter in the Q–U plane is smaller for HSP blazars than for ISP. This also indicates that the polarization plane direction is more stable in HSP sources.

We also found that the rotators seem to be more luminous and more variable in the gamma-ray band than non-rotators. This difference can also be explained by the tendency of the EVPA rotations to occur in LSP sources. These sources have higher luminosities on average than ISP and HSP in the 3FGL because of an instrumental selection effect. The same reason can also explain the increase of their variability indices (Ackermann et al. 2015). For this reason, the optical polarimetry monitoring programmes that select their observing samples on the basis of high variability in the gamma-ray band will observe EVPA rotations more frequently than among blazars on average.

The 180° EVPA ambiguity sets a fundamental limitation on the rate of EVPA rotations that can be detected under a given cadence of observations. So far we have been able to study rotations with rates $\leq$20 deg d^{-1}. There was only one rotation with a rate ∼50 deg d^{-1} detected by *RoboPol*. However, there is an indication in the *RoboPol* data as well as in the literature that fast EVPA rotations with rates 60–130 deg d^{-1} do occur in blazars (e.g. Larionov et al. 2013). We plan to extend our studies to higher rotation rates by increasing our cadence for future monitoring.

ACKNOWLEDGEMENTS

The RoboPol project is a collaboration between the University of Crete/FORTH in Greece, Caltech in the USA, MPIfR in Germany, IUCAA in India and Toruń Centre for Astronomy in Poland. The U. of Crete/FORTH group acknowledges support by the 'RoboPol' project, which is co-funded by the European Social Fund (ESF) and Greek National Resources, and by the European Commission Seventh Framework Programme (FP7) through grants PCIG10-GA-2011-304001 'JetPop' and PIRSES-GA-2012-31578 'EuroCal'. This research was supported in part by NASA grant NNX11A043G and NSF grant AST-1109911, and by the Polish National Science Centre, grant number 2011/01/B/ST9/04618. DB acknowledges support from the St. Petersburg University research grant 6.38.335.2015. KT acknowledges support by the European Commission Seventh Framework Programme (FP7) through the Marie Curie Career Integration Grant PCIG-GA-2011-293531 'SFOnset'. MB acknowledges support from NASA Headquarters under the NASA Earth and Space Science Fellowship Program, grant NNX14AQ07H. TH was supported by the Academy of Finland project number 267324. IM and SK are supported for this research through a stipend from the International Max Planck Research School (IMPRS) for Astronomy and Astrophysics at the Universities of Bonn and Cologne.

REFERENCES

Abazajian K. et al., 2005, AJ, 129, 1755
Acero F. et al., 2015, ApJS, 218, 23
Ackermann M. et al., 2011, ApJ, 743, 171
Ackermann M. et al., 2015, ApJ, 810, 14
Adelman-McCarthy J. K. et al., 2008, ApJS, 175, 297
Angelakis E. et al., 2016, MNRAS, in press
Blandford R. D., Königl A., 1979, ApJ, 232, 34
Blinov D. et al., 2015, MNRAS, 453, 1669 (Paper I)
Blinov D. et al., 2016, MNRAS, 457, 2252 (Paper II)
Brindle C. et al., 1985, MNRAS, 214, 619
Caccianiga A., Maccacaro T., Wolter A., Della Ceca R., Gioia I. M., 2002, ApJ, 566, 181
Ciliegi P., Bassani L., Caroli E., 1993, ApJS, 85, 111
de Grijp M. H. K., Keel W. C., Miley G. K., Goudfrooij P., Lub J., 1992, A&AS, 96, 389
Falco E. E., Kochanek C. S., Muñoz J. A., 1998, ApJ, 494, 47
Fischer J.-U., Hasinger G., Schwope A. D., Brunner H., Boller T., Trümper J., Voges W., Neizvestnyj S., 1998, Astron. Nachr., 319, 347
Giommi P. et al., 1991, ApJ, 378, 77
Giommi P., Piranomonte S., Perri M., Padovani P., 2005, A&A, 434, 385
Henstock D. R., Browne I. W. A., Wilkinson P. N., McMahon R. G., 1997, MNRAS, 290, 380
Hewett P. C., Wild V., 2010, MNRAS, 405, 2302
Hewitt A., Burbidge G., 1987, ApJS, 63, 1
Ho L. C., Kim M., 2009, ApJS, 184, 398
Hovatta T., Valtaoja E., Tornikoski M., Lähteenmäki A., 2009, A&A, 494, 527

Hovatta T. et al., 2014, MNRAS, 439, 690
Hovatta T. et al., 2016, A&A, in press
Hughes P. A., Aller H. D., Aller M. F., 1992, ApJ, 396, 469
Im M., Lee I., Cho Y., Choi C., Ko J., Song M., 2007, ApJ, 664, 64
Jackson N., Browne I. W. A., 1991, MNRAS, 250, 414
Jones D. H. et al., 2009, MNRAS, 399, 683
Junkkarinen V., Hewitt A., Burbidge G., 1991, ApJS, 77, 203
King O. G. et al., 2014, MNRAS, 442, 1706
Larionov V. M. et al., 2013, ApJ, 768, 40
Liodakis I., Pavlidou V., 2015, MNRAS, 454, 1767
Mao P., Urry C. M., Massaro F., Paggi A., Cauteruccio J., Künzel S. R., 2016, ApJS, 224, 26
Marscher A. P. et al., 2008, Nature, 452, 966
Marziani P., Sulentic J. W., Dultzin-Hacyan D., Calvani M., Moles M., 1996, ApJS, 104, 37
Marzke R. O., Huchra J. P., Geller M. J., 1996, AJ, 112, 1803
Meisner A. M., Romani R. W., 2010, ApJ, 712, 14
Meyer E. T., Fossati G., Georganopoulos M., Lister M. L., 2011, ApJ, 740, 98
Murphy D. W., Browne I. W. A., Perley R. A., 1993, MNRAS, 264, 298
Nilsson K., Pursimo T., Heidt J., Takalo L. O., Sillanpää A., Brinkmann W., 2003, A&A, 400, 95
Nolan P. L. et al., 2012, ApJS, 199, 31
Ofek E. O. et al., 2012, PASP, 124, 854
Osmer P. S., Porter A. C., Green R. F., 1994, ApJ, 436, 678
Pavlidou V. et al., 2014, MNRAS, 442, 1693
Pita S. et al., 2014, A&A, 565, A12
Polatidis A. G., Wilkinson P. N., Xu W., Readhead A. C. S., Pearson T. J., Taylor G. B., Vermeulen R. C., 1995, ApJS, 98, 1
Rector T. A., Stocke J. T., 2001, AJ, 122, 565
Richards G. T. et al., 2009a, AJ, 137, 3884
Richards G. T. et al., 2009b, ApJS, 180, 67
Richards J. L. et al., 2011, ApJS, 194, 29
Richards J. L., Hovatta T., Max-Moerbeck W., Pavlidou V., Pearson T. J., Readhead A. C. S., 2014, MNRAS, 438, 3058
Schachter J. F. et al., 1993, ApJ, 412, 541
Schlafly E. F., Finkbeiner D. P., 2011, ApJ, 737, 103
Schmidt M., 1965, ApJ, 141, 1295
Serkowski K., Mathewson D. S., Ford V. L., 1975, ApJ, 196, 261
Shaw M. S., Filippenko A. V., Romani R. W., Cenko S. B., Li W., 2013a, AJ, 146, 127
Shaw M. S. et al., 2013b, ApJ, 764, 135
Snellen I. A. G., Schilizzi R. T., Bremer M. N., Miley G. K., de Bruyn A. G., Röttgering H. J. A., 1999, MNRAS, 307, 149
Sowards-Emmerd D., Romani R. W., Michelson P. F., Healey S. E., Nolan P. L., 2005, ApJ, 626, 95
Stadnik M., Romani R. W., 2014, ApJ, 784, 151
Steidel C. C., Sargent W. L. W., 1991, ApJ, 382, 433
Stickel M., Kuehr H., 1993, A&AS, 100, 395
Stickel M., Kuehr H., 1994, A&AS, 103
Stickel M., Kuehr H., 1996, A&AS, 115, 1
Stickel M., Fried J. W., Kuehr H., 1989, A&AS, 80, 103
Stickel M., Fried J. W., Kuehr H., 1993, A&AS, 98, 393
Thompson D. J., Djorgovski S., de Carvalho R., 1990, PASP, 102, 1235
Vermeulen R. C., Ogle P. M., Tran H. D., Browne I. W. A., Cohen M. H., Readhead A. C. S., Taylor G. B., Goodrich R. W., 1995, ApJ, 452, L5
Veron-Cetty M.-P., Veron P., 1996, A Catalogue of quasars and active nuclei
Wills D., Wills B. J., 1976, ApJS, 31, 143
Wills B. J., Wills D., Breger M., Antonucci R. R. J., Barvainis R., 1992, ApJ, 398, 454
Wright A. E., Ables J. G., Allen D. A., 1983, MNRAS, 205, 793
Zhang H., Deng W., Li H., Böttcher M., 2016, ApJ, 817, 63

APPENDIX A: REDSHIFTS, DOPPLER FACTORS AND SYNCHROTRON PEAK CLASSES

Table A1. Redshifts, Doppler factors and synchrotron peak position classes of the monitored blazars.

Blazar ID RBPL...	Survey name	z	δ^1	Synch. peak class	z ref.	Blazar ID RBPL...	Survey name	z	δ^1	synch. peak class	z ref.
J0017+8135*	S5 0014+81	3.366		LSP	(Osmer, Porter & Green 1994)	J1800+3848*	S4 1758+38	2.092	-	HSP	(Stickel & Kuehr 1994)
J0045+2127^r	GB6J0045+2127	–	–	HSP	–	J1800+7828^r	S5 1803+784	0.684	12.2	LSP	(Rector & Stocke 2001)
J0114+1325	GB6J0114+1325	0.583†	–	ISP	(Stadnik & Romani 2014)	J1806+6949^r	3C 371	0.051	1.1	ISP	(de Grijp et al. 1992)
J0136+4751^r	OC 457	0.859	20.7	LSP	(Hewitt & Burbidge 1987)	J1809+2041^r	RXJ1809.3+2041	–	–	HSP	–
J0211+1051	MG1J021114+1051	0.2†	–	ISP	(Meisner & Romani 2010)	J1813+3144	B2 1811+31	0.117	–	ISP	(Giommi et al. 1991)
J0217+0837	ZS0214+083	0.085	–	LSP	(Shaw et al. 2013b)	J1835+3241*	4C 32.55	0.0579	–	–	(Marzke, Huchra & Geller 1996)
J0259+0747^r	PKS 0256+075	0.893	–	LSP	(Murphy, Browne & Perley 1993)	J1836+3136^r	RXJ1836.2+3136	–	–	ISP	–
J0303−2407	PKS 0301−243	0.2657	–	HSP	(Pita et al. 2014)	J1838+4802	GB6J1838+4802	0.3†	–	HSP	(Nilsson et al. 2003)
J0405−1308	PKS 0403−13	0.5706	–	ISP	(Marziani et al. 1996)	J1841+3218	RXJ1841.7+3218	–	–	HSP	–
J0423−0120	PKS 0420−01	0.9161	19.9	LSP	(Jones et al. 2009)	J1854+7351*	S5 1856+73	0.461	–	LSP	(Henstock et al. 1997)
J0642+6758*	S4 0636+68	3.18	–	LSP	(Osmer et al. 1994)	J1903+5540	TXS1902+556	0.58†	–	ISP	(Meisner & Romani 2010)
J0825+6157*	TXS0821+621	0.542	–	LSP	(Hewitt & Burbidge 1987)	J1927+6117^r	S4 1926+61	0.54†	–	LSP	(Meisner & Romani 2010)
J0841+7053	4C 71.07	2.172	16.3	LSP	(Stickel & Kuehr 1993)	J1927+7358*	4C 73.18	0.3021	1.9	LSP	(Marziani et al. 1996)
J0848+6606	GB6J0848+6605	–	–	ISP	–	J1955+5131*	S4 1954+51	1.23	7.4	LSP	(Stickel & Kuehr 1994)
J0854+5757*	4C 58.17	1.3192	–	ISP	(Hewett & Wild 2010)	J1959+6508	1ES 1959+650	0.047	–	HSP	(Schachter et al. 1993)
J0957+5522	4C 55.17	0.8996	–	ISP	(Hewett & Wild 2010)	J2005+7752	S5 2007+77	0.342	7.9	LSP	(Stickel, Fried & Kuehr 1989)
J0958+6533	S4 0954+65	0.368†	6.2	LSP	(Wills et al. 1992)	J2015−0137	PKS 2012−017	–	–	ISP	–
J1037+5711^r	GB6J1037+5711	0.8304†	–	ISP	(Richards et al. 2009a)	J2016−0903	PMNJ2016−0903	0.367	–	ISP	(Ackermann et al. 2011)
J1048+7143^r	S5 1044+71	1.150	–	LSP	(Polatidis et al. 1995)	J2016+1632*	TXS 2013+163	–	–	–	–
J1058+5628	TXS1055+567	0.143†	–	HSP	(Shaw et al. 2013b)	J2022+7611^r	S5 2023+760	0.594	–	ISP	(Ackermann et al. 2011)
J1203+6031	SBS1200+608	0.0656	–	ISP	(Falco, Kochanek & Muñoz 1998)	J2024+1718*	GB6 J2024+1718	1.05	5.8	LSP	(Veron-Cetty & Veron 1996)
J1248+5820	PG 1246+586	0.8474	–	ISP	(Abazajian et al. 2005)	J2030−0622	TXS2027−065	0.667	–	LSP	(Ackermann et al. 2015)
J1512−0905^r	PKS 1510−089	0.360	16.7	LSP	(Thompson, Djorgovski & de Carvalho 1990)	J2033+2146*	4C 21.55	0.1735	–	–	(Im et al. 2007)
J1542+6129	GB6J1542+6129	0.117†	–	ISP	(Meyer et al. 2011)	J2039−1046	TXS2036−109	1.05†	–	LSP	(Shaw et al. 2013a)
J1551+5806*	GB6 J1551+5806	1.324	–	ISP	(Snellen et al. 1999)	J2042+7508*	4C 74.26	0.104	–	–	(Stickel & Kuehr 1996)
J1553+1256	PKS 1551+130	1.308†	–	ISP	(Richards et al. 2014)	J2131−0915	BZB J2131−0915	0.449	–	HSP	(Giommi et al. 2005)
J1555+1111^r	PG 1553+113	0.360†	–	HSP	(Richards et al. 2011)	J2143+1743	OX 169	0.2107	8.8 ± 1.8^2	ISP	(Ho & Kim 2009)
J1558+5625^r	TXS1557+565	0.300†	–	ISP	(Falco et al. 1998)	J2148+0657	4C 6.69	0.999	15.6	LSP	(Steidel & Sargent 1991)
J1603+5730*	4C 57.27	2.4084†	–	ISP	(Junkkarinen, Hewitt & Burbidge 1991)	J2149+0322	PKS B2147+031	–	–	ISP	–
J1604+5714	GB6J1604+5714	0.720	–	ISP	(Falco et al. 1998)	J2150−1410	TXS2147−144	0.229	–	HSP	(Fischer et al. 1998)
J1607+1551	4C 15.54	0.4965†	–	LSP	(Adelman-McCarthy et al. 2008)	J2202+4216^r	BL Lac	0.0686	7.3	LSP	(Vermeulen et al. 1995)
J1624+5652*	7C 1623+5659	0.415†	–	–	(Richards et al. 2009b)	J2225−0457	3C 446	1.404	16.0	LSP	(Wright, Ables & Allen 1983)
J1635+3808^r	4C 38.41	1.8131	21.5	LSP	(Hewett & Wild 2010)	J2232+1143^r	CTA 102	1.037	15.6	LSP	(Schmidt 1965)
J1638+5720*	S4 1637+57	0.7506	14.0	LSP	(Marziani et al. 1996)	J2243+2021^r	RGBJ2243+203	0.39†	–	HSP	(Meisner & Romani 2010)
J1642+3948	3C 345	0.5928	7.8	LSP	(Marziani et al. 1996)	J2251+4030	BZB J2251+4030	0.229	–	ISP	(Ackermann et al. 2011)
J1653+3945	Mkn 501	0.0337	–	HSP	(Stickel, Fried & Kuehr 1993)	J2253+1608^r	3C 454.3	0.859	33.2	LSP	(Jackson & Browne 1991)
J1725+1152	1H 1720+117	0.018†	–	HSP	(Ciliegi, Bassani & Caroli 1993)	J2311+3425^r	B2 2308+34	1.817	–	LSP	(Wills & Wills 1976)
J1748+7005^r	S4 1749+70	0.770	–	LSP	(Hughes, Aller & Aller 1992)	J2334+0736	TXS2331+073	0.401	–	LSP	(Sowards-Emmerd et al. 2005)
J1751+0939^r	OT 081	0.320	12.0	LSP	(Stickel et al. 1993)	J2340+8015	BZB J2340+8015	0.274	–	HSP	(Caccianiga et al. 2002)
J1754+3212	RXJ1754.1+3212	1.09†	–	ISP	(Shaw et al. 2013a)	–	–	–	–	–	–

Notes. * – control sample source; ^{r} – rotator; † – non-spectroscopic z;
[1] from Hovatta et al. (2009) unless other reference is specified; [2] from Liodakis et al. (in preparation).

This paper has been typeset from a TEX/LATEX file prepared by the author.